AD-A109 685 SRI INTERNATIONAL MENLO PARK CA F/G 4/1
EQUATORIAL PLASMA BUBBLES: VERTICALLY ELONGATED WEDGES FROM THE--ETC(U)
APR 81 R T TSUNODA, R C LIVINGSTON DNA001-81-C-0076

UNCLASSIFIED DNA-TR-81-03 NL

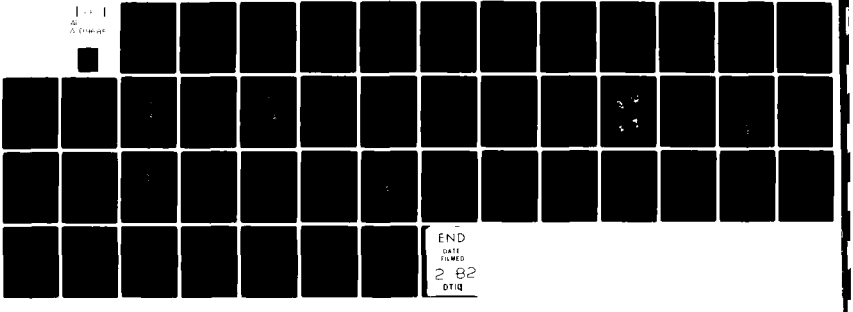

END
DATE FILMED
2 82
DTIC

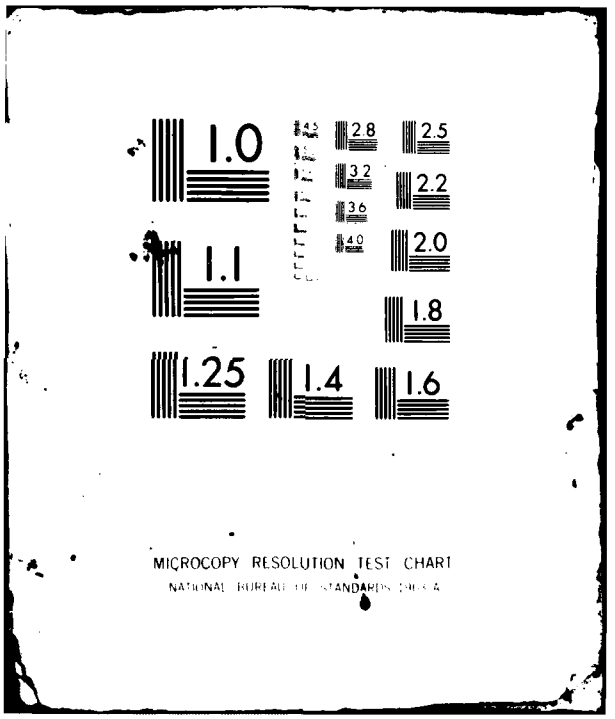
1.0
1.1
1.25
1.4
1.6
1.8
2.0
2.2
2.5
2.8
3.2
3.6
4.0
MICROCOPY RESOLUTION TEST CHART
NATIONAL BUREAU OF STANDARDS 1963-A

LEVEL II

(12)

DNA-TR-81-03

EQUATORIAL PLASMA BUBBLES: VERTICALLY ELONGATED WEDGES FROM THE BOTTOMSIDE F LAYER

Roland T. Tsunoda
Robert C. Livingston
SRI International
333 Ravenswood Avenue
Menlo Park, California 94025

1 April 1981

Technical Report

CONTRACT No. DNA 001-81-C-0076

APPROVED FOR PUBLIC RELEASE;
DISTRIBUTION UNLIMITED.

THIS WORK SPONSORED BY THE DEFENSE NUCLEAR AGENCY
UNDER RDT&E RMSS CODE B322081466 I25AAXHX00002 H2590D.

Prepared for
Director
DEFENSE NUCLEAR AGENCY
Washington, D. C. 20305

Destroy this report when it is no longer needed. Do not return to sender.

PLEASE NOTIFY THE DEFENSE NUCLEAR AGENCY, ATTN: STTI, WASHINGTON, D.C. 20305, IF YOUR ADDRESS IS INCORRECT, IF YOU WISH TO BE DELETED FROM THE DISTRIBUTION LIST, OR IF THE ADDRESSEE IS NO LONGER EMPLOYED BY YOUR ORGANIZATION.

UNCLASSIFIED

SECURITY CLASSIFICATION OF THIS PAGE *(When Data Entered)*

REPORT DOCUMENTATION PAGE		READ INSTRUCTIONS BEFORE COMPLETING FORM
1. REPORT NUMBER DNA-TR-81-03	2. GOVT ACCESSION NO. AD-A109 685	3. RECIPIENT'S CATALOG NUMBER
4. TITLE *(and Subtitle)* EQUATORIAL PLASMA BUBBLES: VERTICALLY ELONGATED WEDGES FROM THE BOTTOMSIDE F LAYER		5. TYPE OF REPORT & PERIOD COVERED Technical Report 6. PERFORMING ORG. REPORT NUMBER SRI Project 2623
7. AUTHOR(s) Roland T. Tsunoda and Robert C. Livingston		8. CONTRACT OR GRANT NUMBER(s) DNA 001-81-C-0076
9. PERFORMING ORGANIZATION NAME AND ADDRESS SRI International 333 Ravenswood Avenue Menlo Park, California 94025		10. PROGRAM ELEMENT, PROJECT, TASK AREA & WORK UNIT NUMBERS Subtask I25AAXHX000-02
11. CONTROLLING OFFICE NAME AND ADDRESS Director Defense Nuclear Agency Washington, D.C. 20305		12. REPORT DATE 1 April 1981 13. NUMBER OF PAGES 48
14. MONITORING AGENCY NAME & ADDRESS*(if different from Controlling Office)*		15. SECURITY CLASS *(of this report)* UNCLASSIFIED 15a. DECLASSIFICATION DOWNGRADING SCHEDULE N/A

16. DISTRIBUTION STATEMENT *(of this Report)*

Approved for public release; distribution unlimited.

17. DISTRIBUTION STATEMENT *(of the abstract entered in Block 20, if different from Report)*

18. SUPPLEMENTARY NOTES

This work sponsored by the Defense Nuclear Agency under RDT&E RMSS Code B322081466 I25AAXHX00002 H2590D.

19. KEY WORDS *(Continue on reverse side if necessary and identify by block number)*

Equatorial spread F
Ionospheric irregularities
Plasma bubbles
Backscatter plumes

20. ABSTRACT *(Continue on reverse side if necessary and identify by block number)*

We address the question regarding the two-dimensional shape of equatorial plasma bubbles in the plane transverse to the geomagnetic field. By comparing the east-west spatial relationship of ion-density depletions measured in-situ by the Atmospheric Explorer-E (AE-E) satellite to backscatter plumes measured by the ALTAIR radar, we show that plasma bubbles are vertically elongated depletions that extend upward from the bottomside of the F layer, in the form of wedges, rather than more isotropically shaped but isolated structures. The shape of plasma bubbles is inferred from (1) ion-density

DD FORM 1 JAN 73 1473 EDITION OF 1 NOV 65 IS OBSOLETE

UNCLASSIFIED

SECURITY CLASSIFICATION OF THIS PAGE *(When Data Entered)*

20. ABSTRACT (Continued)

depletions that exceeded 99 percent in the "neck" regions of plumes, and (2) the eastward drift velocities of the plumes. The expected electrodynamics of vertically elongated plasma bubbles are consistant with the observations of large eastward drift velocities of plumes that are comparable to F-region plasma drift measurements made at Jicamarca and to F-region neutral wind measurements made at Kwajalein. The results also reveal that the west wall of large-scale altitude modulations of the bottomside F layer that produces the primary plumes and bubbles becomes structured, and evolves with the generation of secondary plumes and bubbles.

PREFACE

The authors thank Drs. J. P. McClure and W. B. Hanson (The University of Texas at Dallas) for providing the Atmospheric Explorer-E ion-drift meter data used in this investigation. The data analysis was, in part, supported by National Aeronautics and Space Administration under Contract NAS5-25308 and, in part, by the Defense Nuclear Agency under Contracts DNA001-79-C-0153 and DNA001-81-C-0076.

TABLE OF CONTENTS

LIST OF ILLUSTRATIONS

I INTRODUCTION

A unique feature found to play a major role in the physics of equatorial spread-F (ESF) phenomena is the plasma "bubble". Plasma bubbles are localized depletions in plasma density with spatial dimensions (transverse to the geomagnetic field) on the order of tens to a few hundred km. These dimensions correspond to the outer scale of a spatial irregularity spectrum that falls under the general category of ESF. Because the outer scale of ESF structure (i.e., bubbles) appears to govern the subsequent development and characteristics of the irregularity spectrum, a full description of plasma bubbles can lead to a better understanding of ESF processes.

Plasma bubbles were first discovered by in-situ satellite measurements [Hanson and Sanatani, 1973; McClure et al., 1977], and have since been detected by rocket [Kelley et al., 1976; Morse et al., 1977; Szuszczewicz et al., 1980] and by incoherent-scatter radar [Towle, 1980; Tsunoda, 1980a,b]. The plasma density within bubbles was found to be as much as three orders of magnitude less than the peak plasma density in the F layer (i.e., the depletion can approach 99.9 percent).

Although we now have some idea of bubble size and its percentage depletion, we are less certain about bubble shape. Most direct measurements of plasma bubbles have been one dimensional; e.g., satellite passes through plasma-depleted regions are essentially horizontal, and rocket trajectories are essentially vertical. The only two-dimensional mapping of a bubble to date was made in the meridian plane, i.e., as a function of altitude and geomagnetic latitude, by incoherent-scatter radar [Tsunoda, 1980a]. The mapping of a bubble in that plane supported our expectation that plasma-depleted regions involved whole geomagnetic flux tubes. What is not yet known is the two-dimensional shape of a plasma bubble in the plane transverse to the geomagnetic field.

The two-dimensional shape of plasma bubbles has been predicted by theoretical models of the Rayleigh-Taylor instability. Numerical simulations of the collisional Rayleigh-Taylor instability all show a vertically elongated, plasma-depleted region that extends upward from the bottomside into the topside of the F layer [Scannapieco and Ossakow, 1976; Ossakow et al., 1979; Zalesak and Ossakow, 1980]. The time evolution of bubbles differed, however, depending on the initial perturbation form and possibly other parameters. In some cases, the elongated bubbles "pinched off" into closed depleted regions [Scannapieco and Ossakow, 1976; Zalesak and Ossakow, 1980]. Analyses of the dominant two-dimensional nonlinearity in the Rayleigh-Taylor instability also indicate the development of vertically elongated structures [Chaturvedi and Ossakow, 1977; Hudson, 1978].

Experimental support for these theoretical inferences on bubble shape has been provided in the form of "plumes" observed by backscatter radars [e.g., Woodman and LaHoz, 1976; Tsunoda et al., 1979]. Plumes are regions of strong backscatter (from field-aligned irregularities) that extend upward from the bottomside into the topside of the F layer. The shape of plumes closely resembles the shape of the numerically simulated bubbles. Moreover, plumes have been found to be generally collocated with plasma-depleted regions [Tsunoda and Towle, 1979; Towle, 1980; Tsunoda, 1980a,b; Szuszczewicz et al., 1980].

Although the above evidence favors the existence of highly elongated bubbles, in the form of wedges, that may be "open" in the bottomside F layer (i.e., plasma-density contours in the bubble connect to contours in the bottomside F layer), arguments can be made that suggest the existence of more isotropically shaped bubbles (e.g., circular in the transverse plane) that are "closed" from the bottomside F layer. For example, inferences have been made regarding the shape of bubbles from observed vertical bubble velocities. Bubble velocity is basically proportional to the percentage plasma-density depletion within the bubble, and to its geometric shape [e.g., Ossakow and Chaturvedi, 1978].

Theoretical results of bubble velocity [Ossakow and Chaturvedi, 1978; Ott, 1978; Ossakow et al., 1979] indicate that the vertical bubble velocity computed using more isotropic shapes is in closer agreement with observations [e.g., McClure et al., 1977].

The existence of closed plasma bubbles was made more plausible by Kelley and Ott [1978], who suggested that rising (closed) bubbles leave a trail of turbulent plasma in its wake. Turbulent mixing of inhomogeneous plasma (i.e., with a mean gradient) produces irregularities in plasma density. A backscatter plume can then be interpreted as consisting of a "head" (top portion of plume) that is collocated with a closed bubble and a "neck" (the region connecting the plume head to the bottomside F layer) that is collocated with the turbulent wake of the rising bubble. On the basis of this model, a primary difference between an open and closed bubble model is in the structure of the neck region. In the open bubble model, a large percentage depletion in plasma density is associated with the neck region. But in a closed bubble model, the neck region should be structured (to produce radar backscatter), but should not be significantly depleted in plasma density.

In this paper, we present results that address the question whether the plasma is significantly depleted in the neck region of backscatter plumes. The experiment consisted of comparing plumes as mapped by the ALTAIR radar [Tsunoda et al., 1979; Towle, 1980] with bubbles as measured by an ion-drift meter aboard the NASA Atmospheric Explorer-E (AE-E) satellite. The AE-E satellite was in a low-inclination orbit at an altitude of about 375 km that allowed east-west measurements of bubble characteristics in the neck region of plumes. The results extracted from data collected during July and August 1978 show that the neck region of plumes are indeed highly depleted in plasma density and probably open to the bottomside of the F layer. The results also show that the west wall of large-scale upwellings in the bottomside F layer that produced the primary plumes and bubbles, continues to structure in the form of secondary plumes and bubbles.

II EXPERIMENT

During late July and early August 1978, a coordinated experiment was conducted in the Kwajalein sector to investigate the spatial relationship of plasma bubbles as measured by the AE-E satellite, and backscatter plumes as measured by the ALTAIR radar. ALTAIR is a fully steerable backscatter radar that operates simultaneously at 155.5 MHz (VHF) and 415 MHZ (UHF). We review only the VHF characteristics because only VHF data were used for this analysis. (A brief description of both VHF and UHF system characteristics can be found in Tsunoda et al. [1979] and Towle [1980].) The pulsewidth and beamwidth at VHF were 30 μs and 2.8°, respectively, which gives a range resolution of 4.5 km and a transverse resolution of about 20 km at a range of 400 km. ALTAIR was operated in a "field-perpendicular" scan mode, from west to east in 25 discrete steps that covered a 72° angular sector centered over the radar. In the field-perpendicular mode, the radar beam is directed orthogonally with the geomagnetic field lines at F-region altitudes. Field-perpendicular scans were made successively to map the eastward progression of plumes during the AE-E passes.

The AE-E satellite was in a low inclination orbit so that in-situ measurements aboard AE-E provided information on the east-west (or longitudinal) characteristics of plasma bubbles. During these series of passes over Kwajalein, the AE-E altitude ranged from 372.5 to 374.5 km. The in-situ data used in this analysis consisted of ion-density measurements obtained from the ion-drift meter, log-amplifier output [Hanson and Heelis, 1975]. These data are available with an effective 3-Hz sample rate, which at a satellite velocity of $\sim$ 7.7 km/s amounts to a sample every $\sim$ 2.6 km along the satellite pass. By comparison, the high spatial resolution data from the retarding potential analyzer [e.g., McClure et al., 1977] are sampled approximately every 35 m. But for our purposes, the coarse-resolution data are adequate.

The basic procedure used to compare AE-E data to ALTAIR data was to determine the locations of bubbles relative to the ESF backscatter features, in particular, plumes. Because the AE-E and ALTAIR data were not taken simultaneously, nor instantaneously over the spatial sector containing the bubbles and plumes, temporal and spatial extrapolations were required to compare the data sets. The largest errors are introduced into the estimates of bubble and plume locations by the temporal extrapolation. The spatial extrapolation, along geomagnetic field lines, essentially amounted to a change in the effective altitude of the in-situ measurement through plume features. (The spatial extrapolation is described in more detail in the following section.)

Estimates of the errors introduced by the temporal extrapolation can be made. The references used in the extrapolation are the time of crossing of the ALTAIR magnetic meridian and the eastward drift velocity of plumes and bubbles. For example, ALTAIR completes its scan in about eight min. The scan, centered on the ALTAIR magnetic meridian, therefore, maps ESF backscatter features, e.g., plumes, in east-west direction, which were observed up to ± 4 min from the time of the meridian crossing. A plume drifting at 12 km/min (maximum velocity observed in the data sets) will have changed its east-west position by ± 48 km when referenced to the time of meridian crossing. The AE-E satellite, on the other hand, covers the 560-km east-west sector (at 400-km altitude) over ALTAIR in slightly over a minute. A bubble drifting at 12 km/min will have changed its east-west position by ± 6 km when referenced to the ALTAIR meridian crossing. Because both AE-E and ALTAIR scan from west-to-east, the errors subtract resulting in a net, maximum scan error of about ± 40 km.

III RESULTS

Three selected data sets are presented. The in-situ ion density measurements for all three cases contain depletions that will be interpreted as typical bubble signatures, with maximum percentage depletions of about 99 percent. The results are presented in order of local solar time (LST); the earliest event occurred around 2150 LST [1040 Universal Time (UT)] and the latest event occurred around 2310 LST (1200 UT). The ordering by local time also resulted in the ordering of the plumes that correspond to the plasma bubbles by backscatter strength. The strongest and most altitude-extended plume occurred early in the evening followed by plumes that were weaker in backscatter strength and less altitude-extended. Note that the plume characteristics reflect the growth and decay of individual plumes rather than overall ESF activity on a given night [Tsunoda, 1980c].

A. 13 August 1978 (1041 to 1043 UT)

The ionospheric conditions on this night were characterized by moderate ESF activity. ALTAIR was operated in east-west field-perpendicular scans during two periods, from 1910 to 2010 EST (0800 to 0900 UT) and from 2110 to 2310 LST (1000 to 1200 UT). During the first period, the radar detected only bottomside ESF backscatter associated with the bottomside of the F layer, which rose from around 250-km to 300-km altitude. When ALTAIR was turned back on at 2110 LST (1000 UT), a strong backscatter plume was observed overhead. The second period was characterized by the passage of only two plumes over ALTAIR, the second coinciding with the passage of AE-E through the ALTAIR magnetic meridian. The eastward drift of the backscatter plume around this time (estimated from displacements in ESF backscatter features in successive ALTAIR maps) was approximately 12 km/min (200 m/s), the largest among

the plume drifts found in the three data sets. By 1120 UT, the F layer had returned to 250-km altitude, accompanied only by bottomside ESF backscatter.

The radar-satellite geometry during the AE-E pass (Orbit No. 15199) is shown in Figure 1. The subsatellite track is drawn with circles connected by a solid curve. The circles, given at 16-s intervals, are labeled with the times for those satellite positions. From the times shown, we see that the AE-E pass followed a west-to-east path that was nearly parallel to the zero magnetic-aspect (B_1) curve for ALTAIR, but was displaced about 350 km poleward). The local time corresponding to the AE-E crossing of the ALTAIR magnetic meridian (8.5° true azimuth) was 2151:57 LST (1041:57 UT). The ALTAIR scan, closest in time to the AE-E pass, crossed the magnetic meridian at 2152:19 LST (1042:19 UT) only 22 s after the satellite pass, thus requiring almost no time extrapolation for the data comparison.

To compare the in-situ ion-density and radar backscatter measurements, we spatially extrapolated the variations in ion density along geomagnetic field lines into the plane scanned by ALTAIR. The latitudinal extrapolation (along the dashed lines in Figure 1) amounted to about 3°. Structure in ion density variations with a scale size of greater than a few kilometers should map along geomagnetic field lines with virtually no distortion, because field lines at those scale sizes can be considered as equipotentials [e.g., Farley, 1960]. Tsunoda [1980a], for example, showed that a plasma bubble mapped over at least 10° of latitude. The primary effect of the spatial extrapolation, then, was to raise the effective altitude of the in-situ measurements by 60 to 75 km.

The ion-density data, after spatial extrapolation, is shown plotted along the ALTAIR zero magnetic aspect curve in Figure 1. Note (as shown by the ordinate scale) that depletions or decreasing ion density is plotted upward. Two major disturbed regions are seen: one centered in the vicinity of Kwajalein, and another to the east of

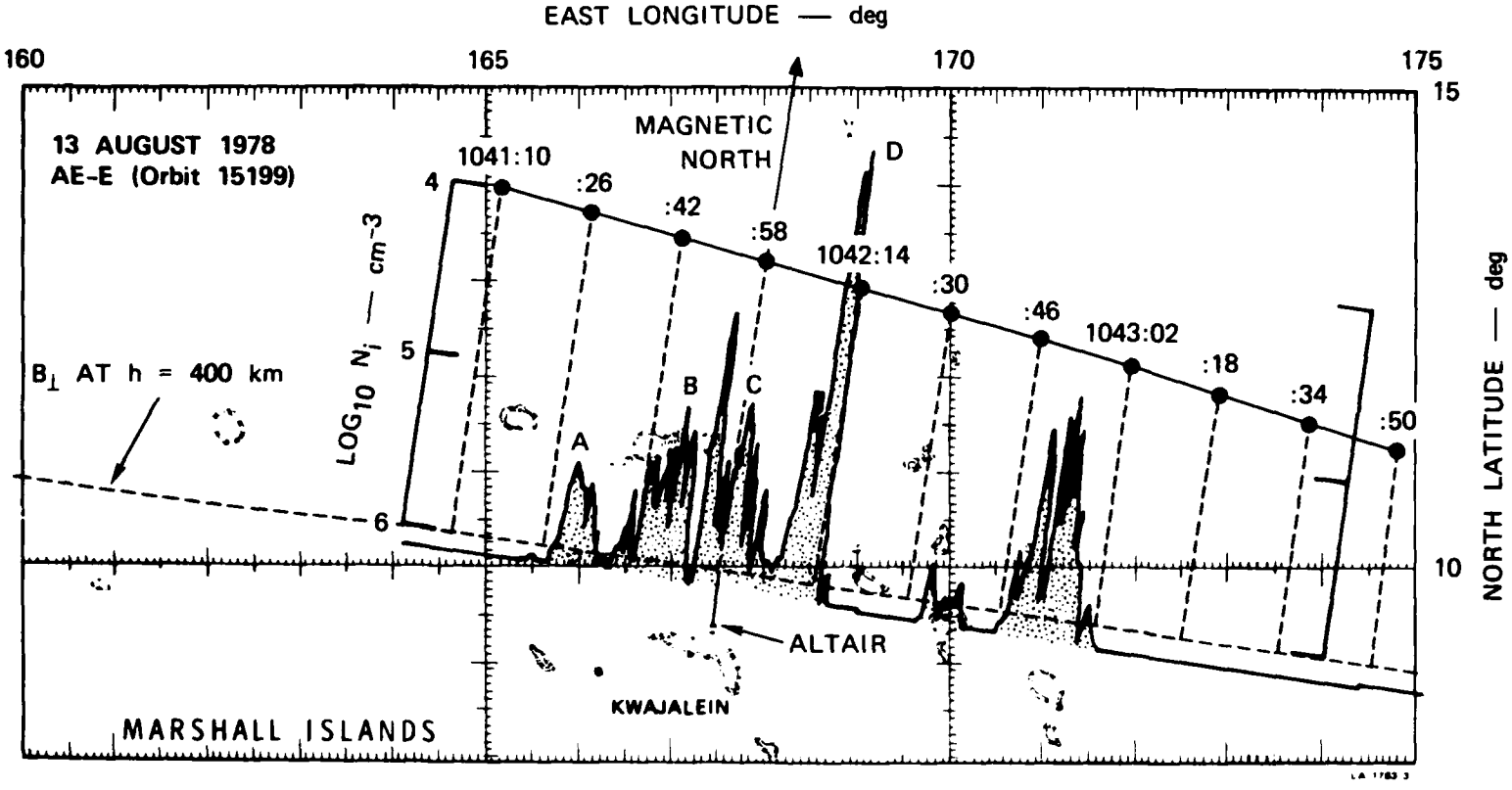

FIGURE 1 RADAR-SATELLITE GEOMETRY ON 13 AUGUST 1978, 1041 TO 1043 UT (AE-E ORBIT NO. 15199)

Kwajalein. For the comparison, we are only interested in the disturbance that extends over a 330-km east-west distance near Kwajalein. We have identified ion-density variations of interest in terms of four depletions, or bubbles, labeled A through D. A distinquishing characteristic of these bubbles is the monotonically increasing depth of depletion associated with the bubble sequence, A through D. Bubble D is depleted by more than two orders of magnitude from the ambient plasma density, much more than the other adjacent bubbles.

The plume-bubble comparison is presented in Figure 2. The ion-density variations are shown in the upper panel (inverted from those presented in Figure 1), and the corresponding ALTAIR backscatter map is shown in the lower panel. The extrapolated altitude of AE-E, as a function of east-west distance from ALTAIR, is shown superimposed on the backscatter map. The map in Figure 2 was constructed by overlapping three maps, each displaced in east-west distance from one another by using a time-to-space conversion based on an estimated drift velocity of the plume seen in the maps. The start time of each map is given along its left (west) edge. The maps are drawn with contours of constant backscatter strength (after range-squared correction) that are referenced to incoherent-scatter (IS) levels. That is, zero dB corresponds to equivalent IS returns from an electron density of 10^6 el/cm^3.

Two backscatter plumes are seen over ALTAIR at the time of the AE-E pass: a major plume that extends upward in altitude to greater than 700 km, and a minor plume that appears next to the west side of the major plume. Bottomside backscatter, which occurs on both sides of the plume pair, tilts upward in the direction of the plumes. Because bottomside backscatter occurs along the bottomside gradient of the F layer [e.g., Szuszczewicz et al., 1980; Tsunoda, 1980b], the shape of the bottomside backscatter implies that the plume pair is associated with a large-scale upwelling that has an east-west dimension of approximately 400 km, or more. An association of plumes and upwellings has been suggested by Tsunoda [1981] and verified by Tsunoda and White [1981]. The AE-E measurements correspond to an west-to-east cut

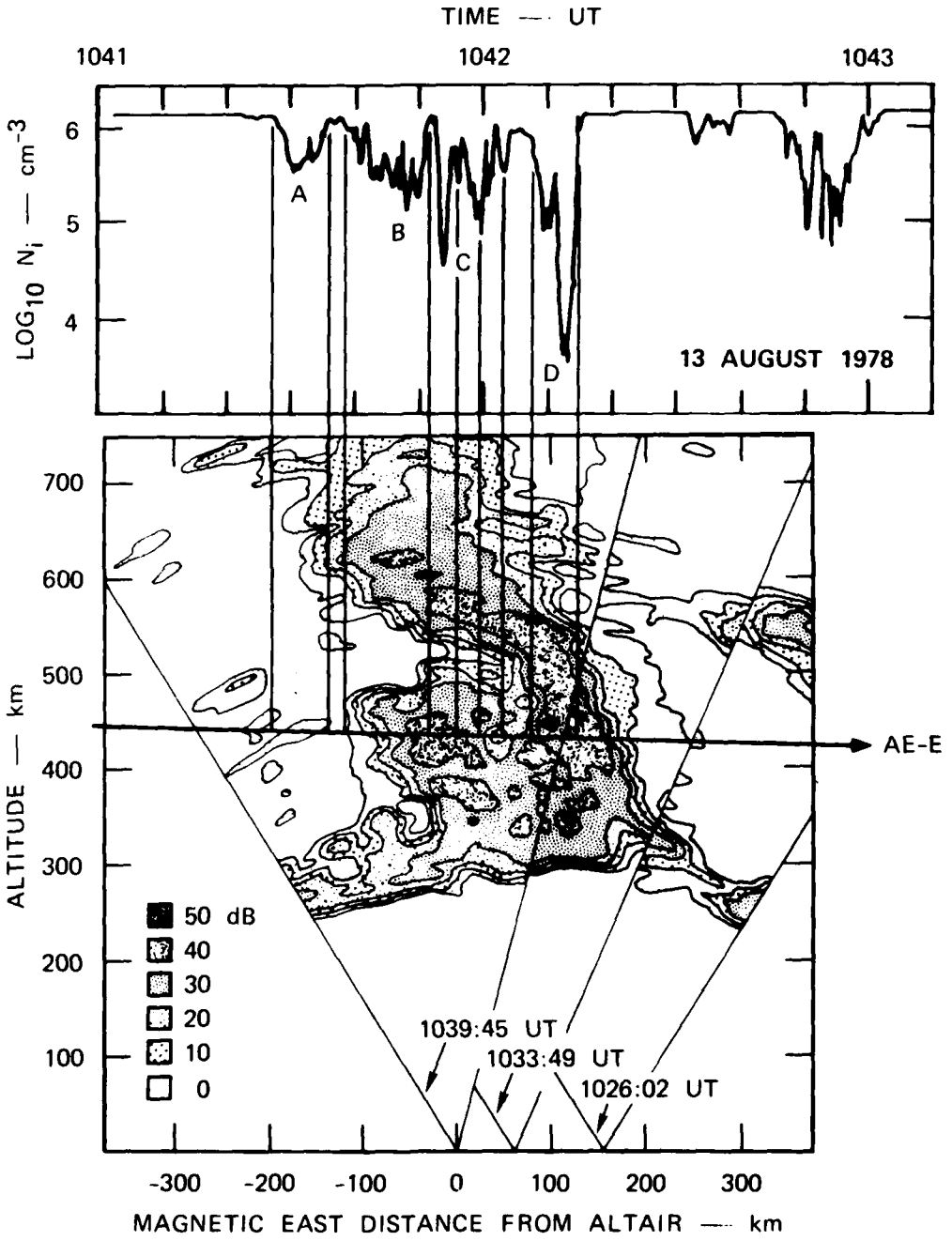

FIGURE 2 SPATIAL RELATIONSHIP OF PLASMA BUBBLES AND ESF BACKSCATTER FEATURES, 13 AUGUST 1978, 1041 TO 1043 UT

through (1) weak patchy backscatter west of the minor plume, (2) the center of the minor plume, and (3) the neck of the major plume.

The relationship of bubbles and plumes can be determined by following the vertical lines between the upper and lower panels in Figure 2. Bubble A corresponds to the weak patchy backscatter region located to the west of the minor plume. The weak backscatter might be associated with the relative absence of structure within Bubble A. The more structured Bubbles B and C correspond to the west and east halves of the minor plume. And finally, Bubble D corresponds with the strongest backscatter region in the neck of the major plume. The general collocation of backscatter and bubbles found in Figure 2 breaks down only when comparing Bubble D to the east side of the major plume, as constructed from the second and third ALTAIR maps. The discrepancy is attributed to the longer time extrapolation required for comparison of the AE-E data to the backscatter found in the second and third maps. The key result of the data comparison is the finding that the largest percentage depletion (Bubble D) occurred in the neck of the major plume. These results suggest that the geometric shape of plasma bubbles are vertically elongated, highly depleted structures.

Further insight into the actual shape of the plasma depletion in the neck of the major plume can be obtained by comparing AE-E measurements made during two successive orbits. A second AE-E measurement was made (Orbit No. 15200) of the same plasma-depleted regions described in Figures 1 and 2. During the second pass through the bubbles of interest (1221 to 1223 UT), AE-E was located approximately 8° further south in magnetic dip latitude from that during the first pass. For a nominal magnetic dip of 9°, the latitude difference transposes into an altitude difference of about 140 km. The second pass, therefore, intersected the plasma-depleted region at a lower altitude, perhaps 100 km below the first pass if we account for a descending F layer during this period. (The peak of the F layer was at approximately 400-km altitude during the first pass and at about 350-km altitude during the second pass.)

The ion-density measurements of the bubble region made during the two AE-E passes are presented in Figure 3. The data from the second pass is shown below those from the first pass. The left ordinate gives the ion-density scale for the second pass; it is displaced downward by one decade from the ion-density scale for the first pass (right ordinate). The time coordinates are arbitrarily aligned, simply to show the relationship of similar features observed during the two passes.

Two basic differences can be found between the ion-density measurements made during the two passes. First, the plasma depletion measured during the second pass corresponds to Bubbles C and D only. There is no evidence during the second pass of Bubbles A and B. And second, the depth of the plasma-depleted regions in the second pass is much larger than that found in corresponding regions in the first pass.

A two-dimensional shape of the plasma-depleted region that can account for these observations is presented in Figure 4. The bubbles are shown as two plasma-depleted wedges that extend upward from near the crest of a single, large upwelling of the bottomside F layer. Separate large-scale upwellings of the bottomside F layer do not seem to be associated with each bubble, as indicated by the fact that the ion density between Bubbles C and D did not recover to ambient levels. Bubble D corresponds to the primary wedge that is usually generated from near the crest of the large-scale upwellings [e.g., Tsunoda and White, 1981], depicted in Figure 4 by the lowest dashed contour of constant plasma density. Bubbles B and C can be interpreted as bifurcated segments of a single wedge that developed from the west wall of the large-scale altitude modulation. And finally, Bubble A might be a remnant of an old bubble or a fragment associated with Bubbles C and B.

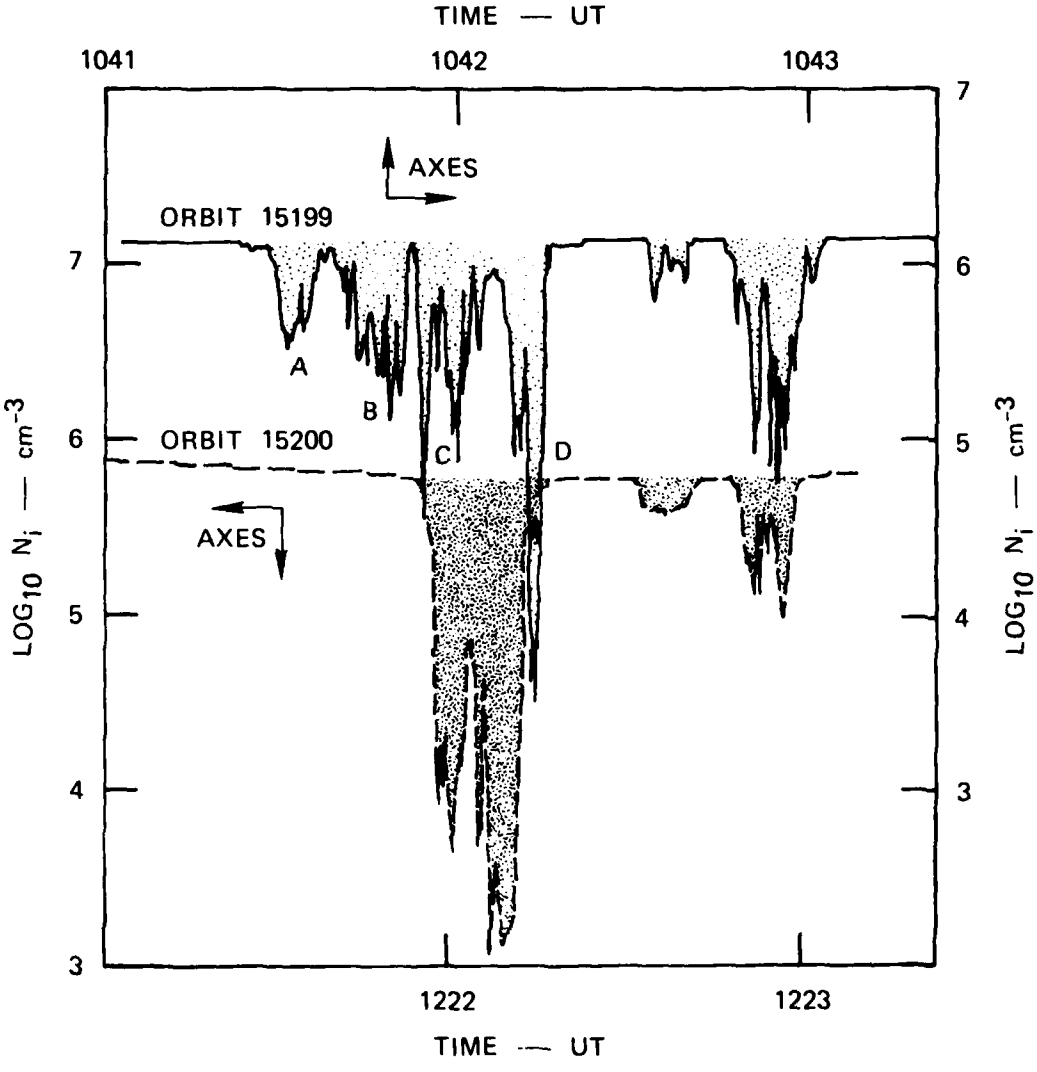

FIGURE 3 **AE-E ION-DENSITY MEASUREMENTS OF THE SAME PLASMA BUBBLES OBTAINED DURING TWO CONSECUTIVE PASSES, 13 AUGUST 1978**

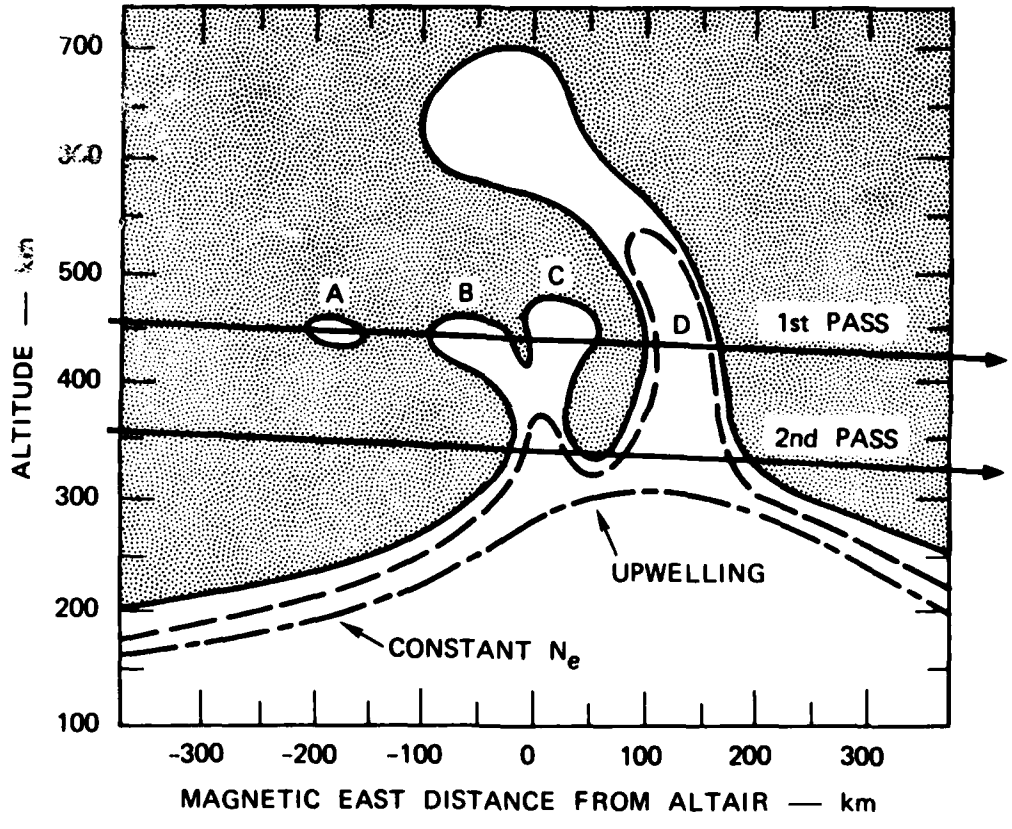

FIGURE 4 A TWO-DIMENSIONAL MODEL OF THE PLASMA-DEPLETED REGION ASSOCIATED WITH FIGURE 2 (13 AUGUST 1978)

The AE-E measurements made during the two passes are also consistent with this model. During the first pass, the AE-E satellite intersected the four bubble features, as described earlier and shown in Figure 4. The second pass can be interpreted as having intersected the neck regions of both major and minor plumes. Because of its lower altitude, the satellite crossed contours of lower plasma density than that intersected during the first pass. The measurement of larger plasma depletions at lower altitudes is consistent with the concept that plasma is drawn up from the lower ionosphere by large-scale electric fields that develop within the upwelling via the collisional Rayleigh-Taylor and gradient-drift instabilities [e.g., Zalesak and Ossakow, 1980]. The absence of a depleted region beneath Bubble A and between Bubbles A and B may suggest that depleted regions can "pinch off" into closed depleted regions.

The bifurcation of the minor wedge also is consistent with the development of a plasma bubble via the aforementioned instabilities. Structuring is expected to occur along the top wall of the plasma bubble, or wedge, during its development. Figure 5 shows that the minor wedge is in its growth phase during this event. The sequence of ALTAIR maps taken just prior to the first AE-E pass showed the upward development of the minor plume (as the backscatter structures drift eastward). The minor plume is clearly seen (40-dB contour) in Figure 5(b) with the top of the plume located at 420-km altitude. In Figures 5(c) and 5(d), the top of the plume is located at 440 km and 480 km, respectively. In contrast the major plume was nearly fully grown during this time period. The high degree of structure found in Bubbles B and C, compared to Bubble D, suggests that more structure is associated with a developing bubble than a fully grown bubble.

B. 31 July 1978 (1130 to 1132 UT)

The ionospheric conditions on this night were similar to those for the first data set. Bottomside ESF backscatter was observed between 1940 LST (0830 UT) and 2110 LST (1000 UT), with the bottomside

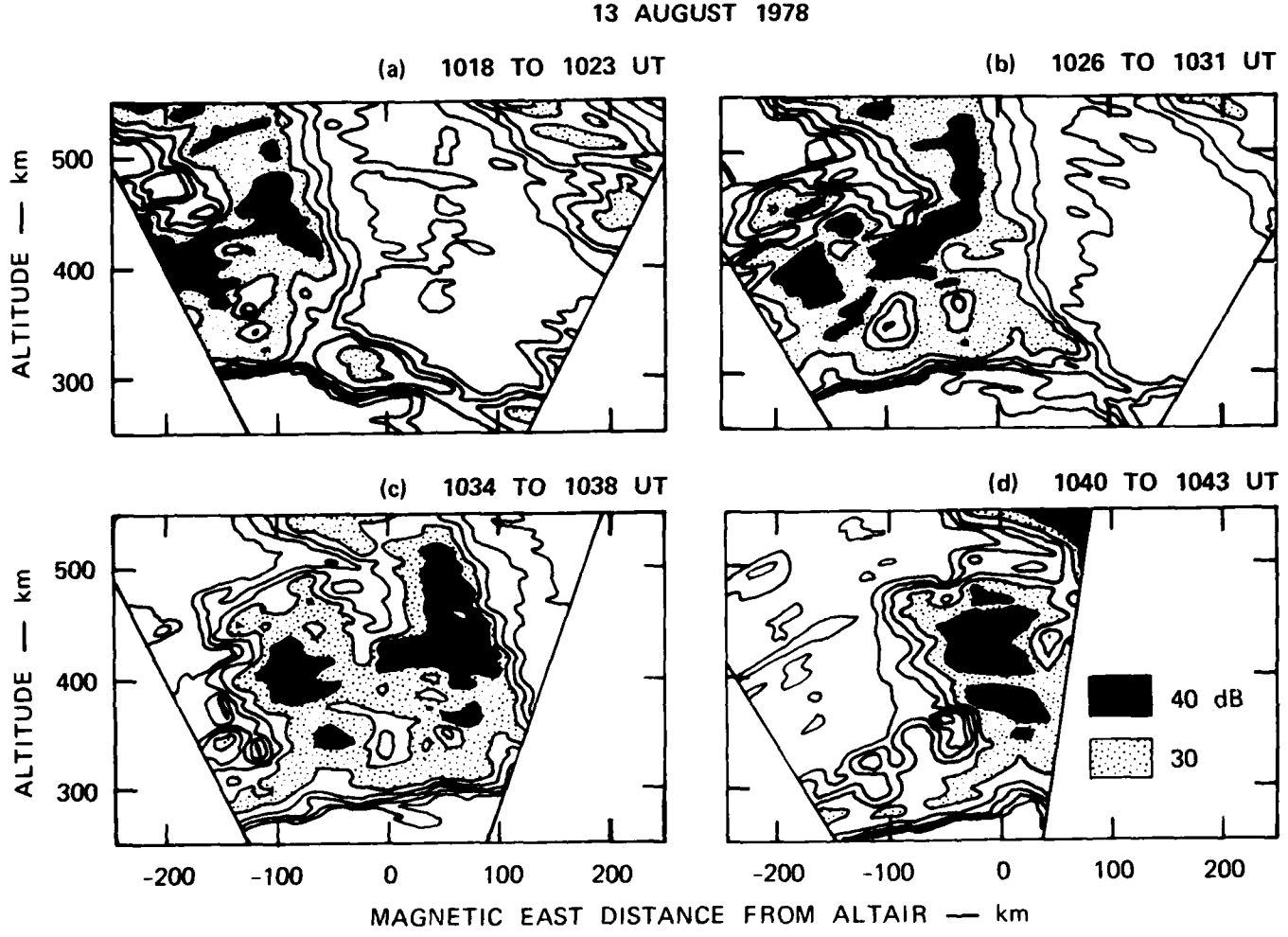

FIGURE 5 TIME-SEQUENCED ALTAIR MAPS SHOWING THE GROWTH OF THE SECONDARY PLUME IN FIGURE 2 (13 AUGUST 1978)

of the F layer located around 250-km altitude. Plumes were observed over ALTAIR from 2110 LST (1000 UT) through the period of the AE-E pass. At the time of the satellite pass, a plume was observed to the east of ALTAIR, in its decay phase. The eastward plume drift was approximately 9 km/min (150 m/s), the lowest drift velocity observed during the three nights reported in this paper. Two more strong plumes were observed over ALTAIR after the AE-E pass, between 2240 LST (1130 UT) and 2340 LST (1230 UT) when ALTAIR was turned off.

The radar-satellite geometry during the AE-E pass (Orbit No. 14996) is shown in Figure 6. The subsatellite track, again drawn with circles connected by a solid curve, is seen to extend from west to northeast of Kwajalein crossing the ALTAIR magnetic meridian about 360 km to the north of the radar. The time of the meridian crossing was 2241:00 LST (1131:00 UT), 51 min later than that for the first data set. The ALTAIR scan crossed the magnetic meridian at 2244:53 LST (1134:53 UT), 3 min 53 s after the AE-E meridian crossing.

The ion-density measurements, after spatial extrapolation, are also shown plotted in Figure 6 along the ALTAIR zero magnetic-aspect contour. The ion-density variations can be interpreted as a long train of plasma bubbles that extends over a broad longitudinal sector. Although there is no obvious periodicity associated with the bubble train, the bubbles are spaced a few hundred kilometers from one another. A more apparent characteristic is the amount of structure associated with each bubble. Clearly, the bubbles that occurred to the west of Kwajalein are more structured than the bubbles that occurred to the east of Kwajalein; a feature that is consistent with the generation and growth of bubbles earlier in the night followed by bubble decay (as they drift eastward). The bubbles of interest, labeled A through D, are those containing less structure, a characteristic we associate with decaying bubbles. Of the labeled bubbles, Bubbles C and D are closely spaced and perhaps part of the same disturbance, but Bubbles A and B are widely spaced and are clearly independent features.

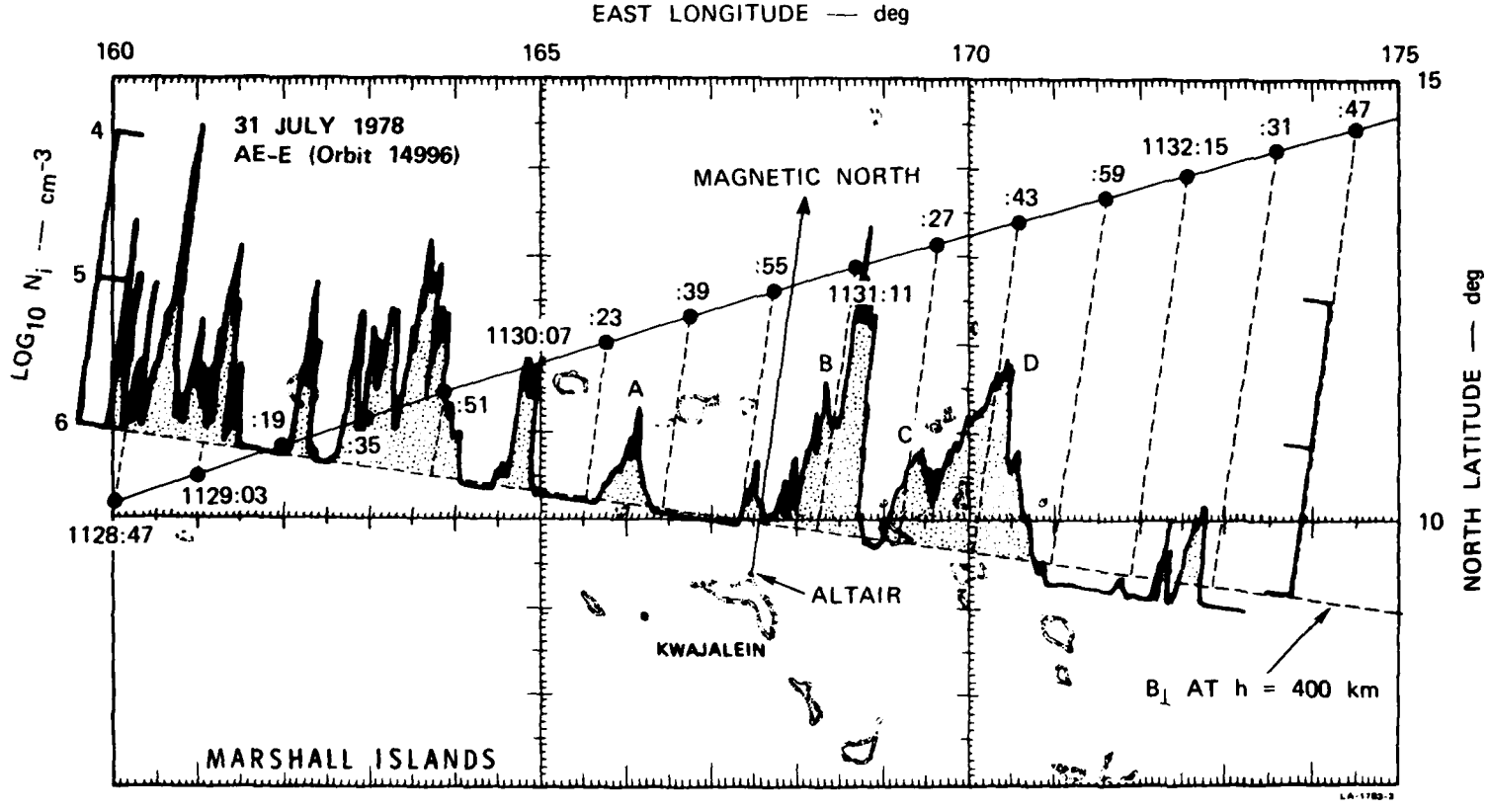

FIGURE 6 RADAR-SATELLITE GEOMETRY ON 31 JULY 1978, 1130 TO 1132 UT (AE-E ORBIT NO. 14996)

The plume-bubble comparison is presented in Figure 7. The ion density data are presented in the upper panel, and the backscatter data are presented in the lower panel. Comparison of pertinent features can be made by following the vertical lines connecting the two data sets. The equivalent satellite altitude in the plane of the ALTAIR scan is seen to increase as the satellite passed from west to east, because of the spatial extrapolation.

Bubble A is seen to correspond to a region of virtually no ESF backscatter. The depletion, however, is clearly aligned with a small plume located directly beneath it. We interpret the small plume as the remnant neck region of a larger plume, whose portion in the topside F layer had already gone through its decay phase [Tsunoda, 1980c]. The structured 0-dB backscatter contour that remains above the small plume suggests that the plume probably had extended up to 550 km. The relative absence of structure in Bubble A is consistent with the absence of ESF backscatter.

Bubble B is similar in shape to the composite shape produced by Bubbles B, C, and D in the first data set. That is, Bubble B is characterized by (1) a structured west wall with depletions that are relatively shallow, (2) a deep narrow depletion that might be considered the center of the bubble, and (3) a steep, relatively unstructured east wall. This bubble signature corresponds in space to a large, but decaying plume. The AE-E measurement appears to have been made through the neck region or very close to the head of the plume. The west wall of Bubble B corresponds to relatively weak (0 to 10 dB), but structured ESF backscatter. The center of the bubble appears to be offset slightly to the west of the neck of the plume. The offset is expected (see Section II) because of the finite time of the ALTAIR scan, which allowed the plume to drift eastward beyond its actual position at the time of the AE-E bubble measurement. We, therefore, conclude that the major depletion in Bubble B was probably aligned with the strongest backscatter region in the neck of the plume.

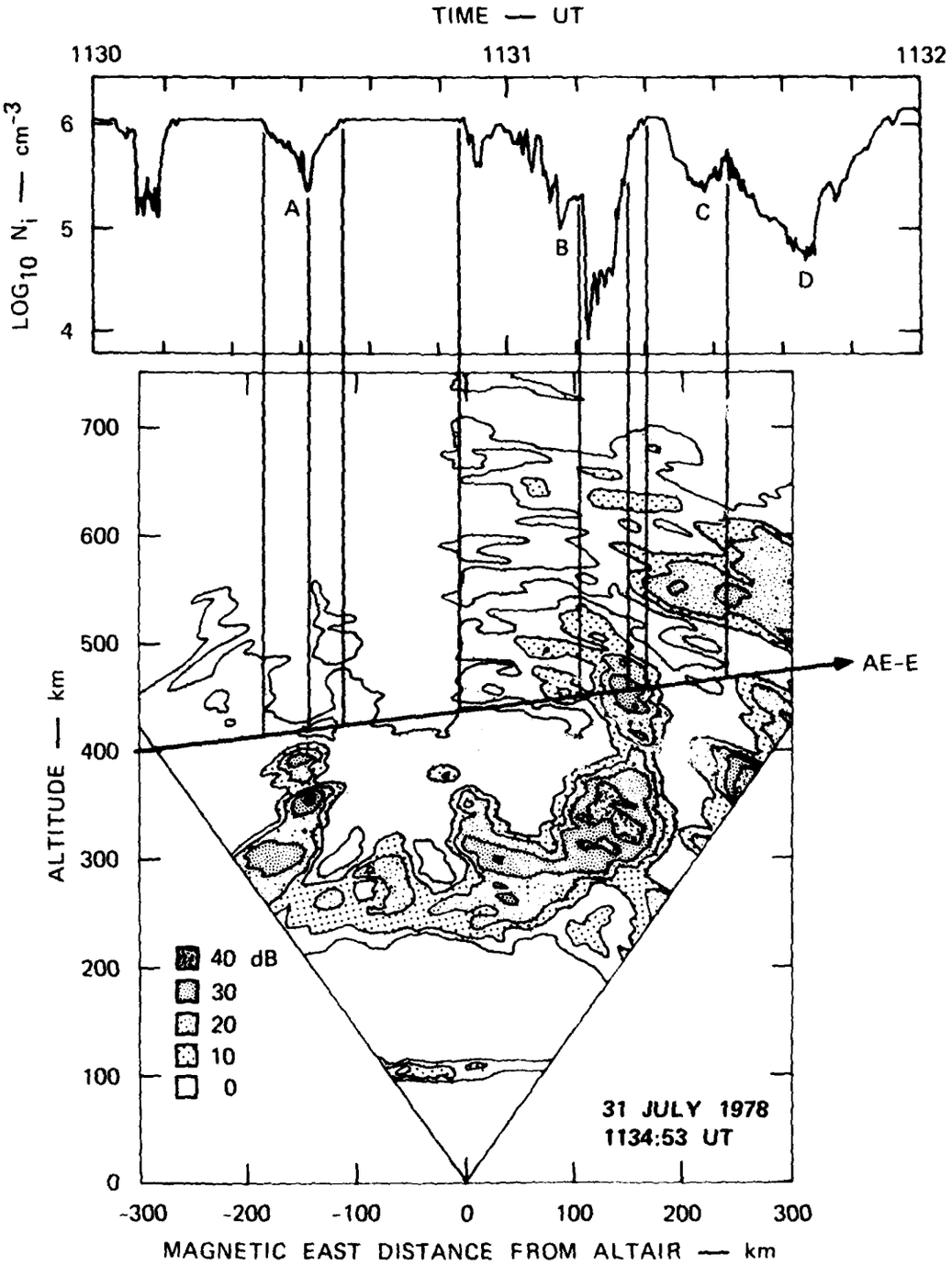

FIGURE 7 SPATIAL RELATIONSHIP OF PLASMA BUBBLES AND ESF BACKSCATTER FEATURES, 31 JULY 1978, 1130 TO 1132 UT

Bubbles C and D appear to have a similar spatial relationship with a plume that can be seen along the east edge of the scanned sector. Bubble C is associated with a structured west wall, or perhaps with a turbulent region between the two plumes. Bubble D can be interpreted as the center of the bubble and probably to the neck or head region of the east plume.

Implicit in the spatial relationship of Bubble B to the neck region of the major plume and to the decaying ESF backscatter is that the depth of the structure along the west wall of Bubble B is shallow. Because F-region plasma is considered incompressible, the shallow depth of the structure implies that the structuring did not involve highly depleted regions such as the central portion of the neck region; instead, it is consistent with the concept of a local structuring of the west wall of the bubble.

C. 29 July 1978 (1159 to 1202 UT)

ALTAIR was operated from about 1925 to 2340 LST (0815 to 1230 UT) on this night. Bottomside ESF backscatter commenced around 1955 LST (0845 UT) with the bottomside of the F layer located around 300-km altitude. Although a plume developed around 2040 LST (0930 UT) to the east of ALTAIR, ESF plume activity did not fully develop until 2200 LST (1050 UT) when a plume was observed to the west of ALTAIR. (ALTAIR was not operated from 1050 to 1150 UT.) The plume sighted at 2200 LST (1050 UT) was apparently the lead plume associated with a longitudinally extended region of disturbance. At the time of the AE-E pass, the tail end of the disturbed region was situated over ALTAIR. The eastward plume drift was approximately 11 km/min (183 m/s), slightly less than that computed for the first event.

The radar-satellite geometry during the AE-E pass (Orbit No. 14965) is shown in Figure 8. The subsatellite track was from southwest to northeast and passed almost directly over Kwajalein. The local time of the ALTAIR magnetic meridian crossing by AE-E was 2310:26 LST

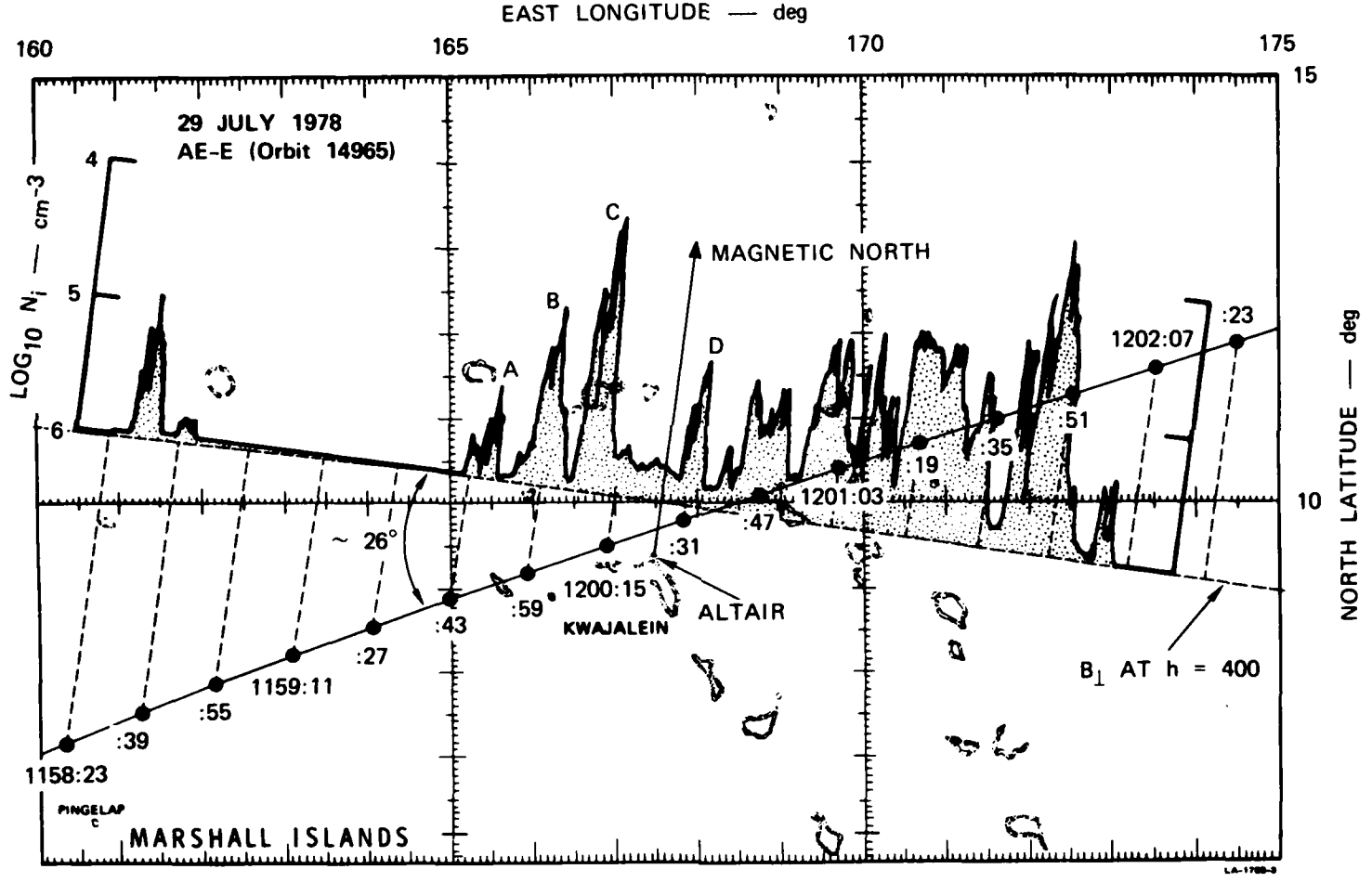

FIGURE 8 RADAR-SATELLITE GEOMETRY ON 29 JULY 1978, 1159 TO 1202 UT (AE-E ORBIT NO. 14965)

(1200:26 UT), the latest in local time of the three data sets. The ALTAIR scan crossed the meridian at 2317:03 LST (1207:03 UT), about 6-1/2 min after the AE-E meridian crossing.

The ion-density data, after spatial extrapolation, are shown plotted along the ALTAIR zero magnetic aspect contour in Figure 8. The disturbed region is virtually continuous and extends over 800 km in east-west direction. The structure associated with the bubbles appears to be comparable to that found in the second data set but less than that found in the first data set. We have again selected four bubbles, labeled A through D, for comparison with the corresponding ALTAIR backscatter data. The selected bubbles are seen to occur on the trailing end of the disturbed region. Bubbles A, B, and C are spaced closely together and have a depletion pattern that is similar to Bubbles A through D in the first data set, and to the shape of Bubble B in the second data set. That is, the depth of the depletions increases from west to east, the depth being least in Bubble A and most in Bubble C. Bubble D in Figure 8 is displaced from the other three bubbles and is not a part of this sequence.

The plume-bubble comparison is presented in Figure 9. We find that Bubbles B and C are associated with two large plumes. The satellite pass is again seen to intersect through the neck regions of the plumes. Although the alignment is not perfect (i.e., strongest backscatter does not always correspond to maximum bubble depletion), clearly the depletions occur in the neck regions of the plumes. Bubble A corresponds to a slightly enhanced backscatter patch, but not to the smaller plume seen along the west edge of the ALTAIR map. If we interpret the small plume as upward-developing, probably, the AE-E measurement was made before the plume reached the altitude of the satellite. With this interpretation, the plasma-bubble relationship is identical with that found in the first data set. The largest depletion, Bubble C, is spatially collocated with the strongest and most altitude-extended plume. A remnant of the head region of this major plume can be seen in the upper left hand corner of the ALTAIR map.

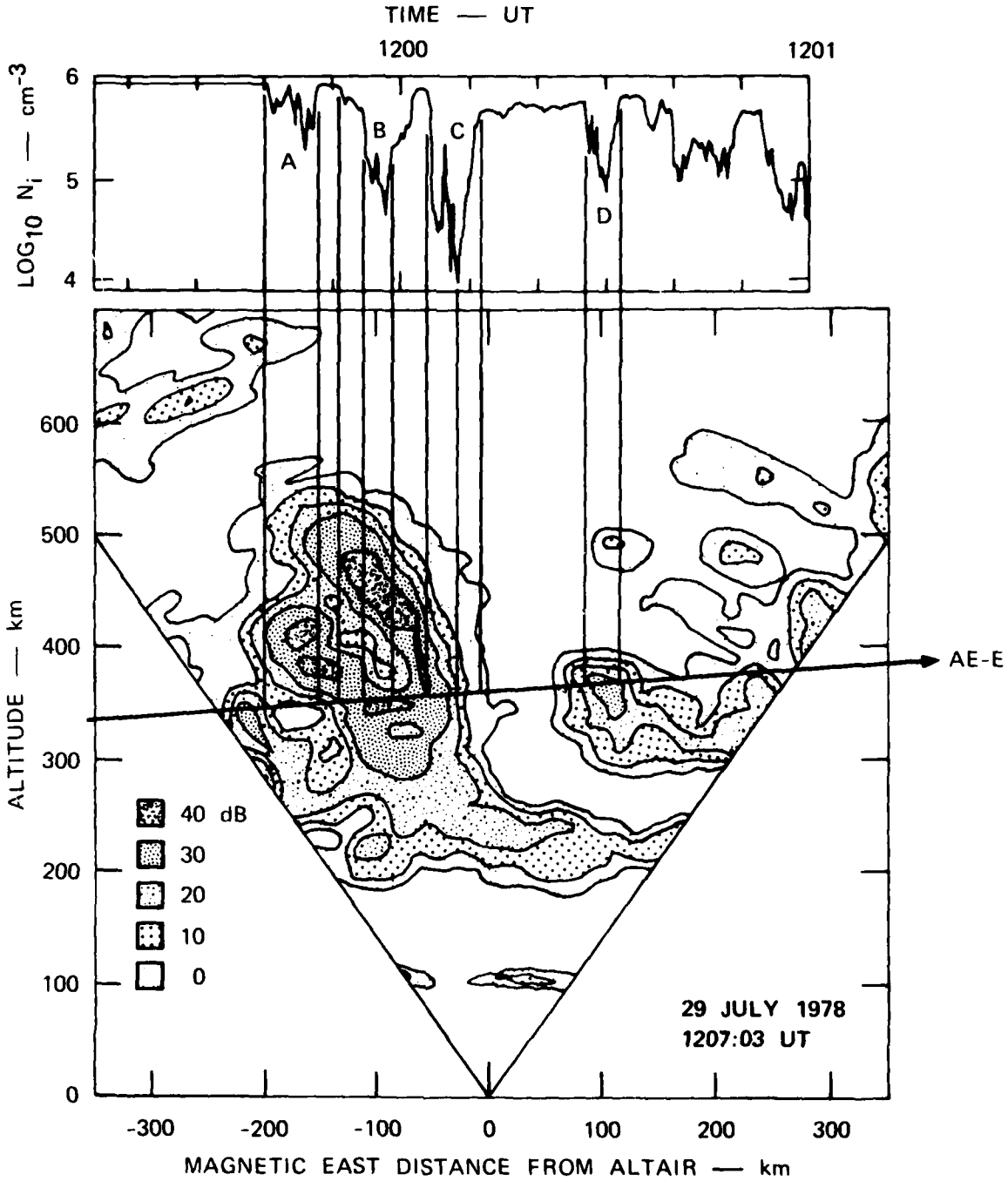

FIGURE 9 SPATIAL RELATIONSHIP OF PLASMA BUBBLES AND ESF BACKSCATTER FEATURES, 29 JULY 1978, 1159 TO 1202 UT

Secondary depletions, Bubbles A and B, are associated with smaller plumes that probably developed along the west wall of a large-scale upwelling in the bottomside F layer.

Bubble D and depletions to the east of it are not associated with the same group of ESF backscatter as the other labeled bubbles. Bubble D, however, is collocated with a trailing edge of a generally disturbed region containing ESF backscatter. The other depletions to the east of Bubble D also appear to coincide with ESF backscatter.

In the first data set, we suggested that the minor plumes (and bubbles) along the west wall of large-scale altitude modulation (in the bottomside of the F layer) develop later than the major plume located at the crest of the altitude modulation. We can also determine the relative ages of Bubbles B and C in this data set by examining a sequence of ALTAIR maps that contain the time evolution of the associated plumes. For this purpose, we have traced the 30- and 40-dB contours that describe the two largest plumes from a sequence of four backscatter maps and superimposed them onto one map, shown in Figure 10. At 1154:40 UT, the time of the first tracing, the major plume was already fully developed, and perhaps already in its decay phase. The decay of the major plume in the 15-min period following the time of the AE-E pass (second tracing) is seen in the third (1214:50 UT) and fourth (1222:30 UT) tracings in Figure 10. If we now examine the time evolution of the secondary plume, we find it still in its growth phase [Tsunoda, 1981]. Although the secondary plume was not visible in the first tracing, its growth is clearly seen in the last three tracings in Figure 10.

A shape of the plasma-depleted region that can account for the observations is shown in Figure 11. Bubble C is shown as a vertically-elongated (and tilted) wedge that originates near the crest of a large-scale altitude modulation. As shown, Bubble C is open to the bottomside of the F layer. We have also assumed in the model that Bubble C

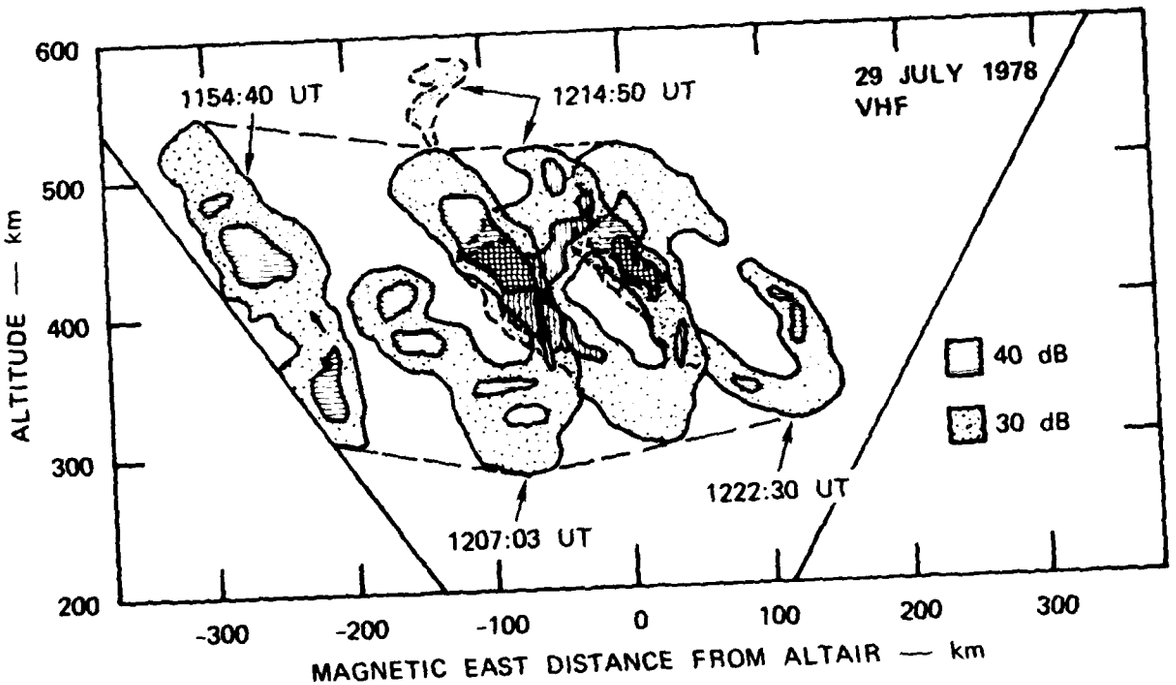

FIGURE 10 TIME SEQUENCE OF ESF BACKSCATTER CONTOURS THAT SHOW THE GROWTH OF THE SECONDARY PLUME (LEFT) AND THE DECAY OF THE PRIMARY PLUME (RIGHT) (29 JULY 1978)

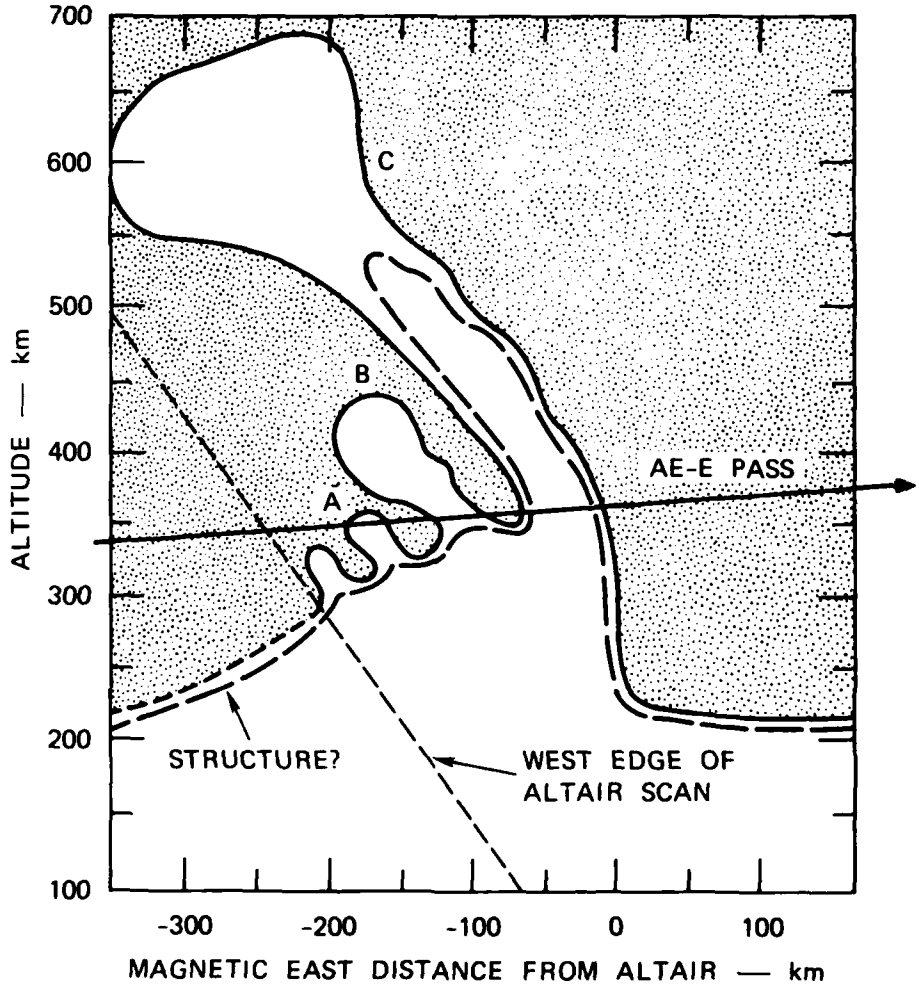

FIGURE 11 A TWO-DIMENSIONAL MODEL OF THE PLASMA-DEPLETED REGION ASSOCIATED WITH FIGURE 9 (29 JULY 1978)

was still connected to the head of the plume at the time of the AE-E pass. It is also possible that the wedge pinched off in the topside F layer.

Bubbles A and B are shown in the model as part of the structuring along the west wall of a large-scale upwelling. We have also included a third wedge to represent the small plume seen along the west edge of the ALTAIR map in Figure 9. Structuring probably continues along the wall to the west side of the ALTAIR scan (dashed line), but we have chosen not to speculate on that structure. It is also possible that the structure there might be quenched by collisions at those low altitudes.

IV DISCUSSION AND CONCLUSIONS

In this paper, we have shown through comparisons of in-situ ion-density measurements and radar backscatter measurements that plumes and bubbles are spatially collocated in the east-west direction. A key result of this analysis is that the neck region of major plumes is associated with plasma-density depletions that can approach three orders of magnitude, i.e., neck-region depletions are comparable to the largest observed bubble depletions [Hanson and Sanatani, 1973; McClure et al., 1977]. This result indicates that the neck is an integral part of the plasma bubble structure and not simply produced by plasma turbulence in the wake of a rapidly-rising, but closed bubble [Kelley and Ott, 1978]. Instead, plasma bubbles are vertically elongated wedges that extend from the bottomside into the topside of the F layer. Furthermore, the bubbles are probably open-ended to the bottomside F layer (e.g., as depicted in Figures 4 and 11).

The general collocation of plumes and bubbles, shown by results presented here and elsewhere [Tsunoda and Towle, 1979; Tsunoda, 1980a, b; Towle, 1980; Szuszczewicz et al., 1980], implies that backscatter-producing irregularities are primarily generated in regions of low plasma density. This preference for low plasma densities is consistent with the production of these irregularities by the lower-hybrid-drift (LHD) instability [Huba et al., 1978; Sperling and Goldman, 1980; Huba and Ossakow, 1981]. For a given gradient scale length in plasma density (associated with the walls of bubbles or with larger-scale irregularities embedded in the bubbles), the growth rate of this instability increases with decreasing plasma density. For example, the LHD instability requires a mean plasma density of less than 10^5 el/cm^3 for a typical gradient scale length around 50 m [e.g., Sperling and Goldman, 1980]. A bubble with associated backscatter, therefore, will have to be 90 percent depleted as it passes through

an F-layer peak with a plasma density of 10^6 el/cm^3. All major plumes and bubbles analyzed in this paper satisfied this depletion requirement.

The conclusion that plasma bubbles are vertically elongated wedges is consistent with the numerical simulations of the nonlinear, collisional Rayleigh-Taylor instability [Scannapieco and Ossakow, 1976]. The vertical elongation is also consistent with bubble shape expected from the two-dimensional nonlinearity in the Rayleigh-Taylor instability that is believed to dominate the bubble development [Chaturvedi and Ossakow, 1977; Hudson, 1978].

Other less direct evidence, in particular the east-west drift velocity of backscatter plumes, can also be used to support the conclusion that bubbles are vertically elongated upwellings. The reasoning is as follows: A bubble, being a depletion, will move faster than the E × B motion of the bulk plasma. Its speed will depend on the percentage depletion and geometric shape of the bubble [e.g., Ossakow and Chaturvedi, 1978]. At night, the bulk plasma motion is eastward (in the ground reference frame), driven by an eastward neutral wind via an F-region dynamo [Rishbeth, 1971]. Because the coupling between the plasma and neutral gas is not perfect, the bulk plasma moves slower than the neutral gas [Rishbeth, 1971; Woodman, 1972]. In the reference frame of the neutral wind, therefore, the bulk plasma is moving westward, which means that in this reference frame, a bubble should move westward faster than the bulk plasma. Woodman and LaHoz [1976], Ossakow and Chaturvedi [1978], and Ott [1978] all suggested that the westward tilt of backscatter plumes could be accounted for by the described process. In other words, highly depleted bubbles if not constrained by their geometric shape, should move very slowly eastward when viewed from the ground reference frame. For example, disregarding bubble shape, a bubble that is 99 per cent depleted should move at 1/100th the bulk plasma drift.

In the three data sets analyzed, we found that the eastward plume drift ranged from 150 m/s to 200 m/s, with a mean speed of 178 m/s. In comparison, the F-region bulk plasma drift was reported not to exceed 135 m/s [Woodman, 1972; Fejer et al., 1981]. Although the difference between plume drift and bulk plasma drift is as much as 48 percent, the difference is not considered to be unreasonable in view of the fact that the measurements were made at significantly different longitudes. The plume drift is certainly not small compared to the F-region bulk plasma drift. On this basis, we would conclude that the plume drift is comparable to F-region bulk plasma drift.

A more appropriate comparison is between plume drift and F-region neutral winds measured over Kwajalein. The first reports of neutral winds over Kwajalein in 1977 indicate that the wind speed did not exceed 150 m/s [Sipler and Biondi, 1978]. Although the plume drift (for 1978) is larger than the measured neutral winds (for 1977), the difference is less than 20 percent. We conclude from this relatively small difference that the percentage depletion in bubbles does not control the east-west plume drift.

The other factor that controls bubble velocity is the bubble shape, i.e., its axial ratio [Ossakow and Chaturvedi, 1978]. Bubble velocity decreases in the direction perpendicular to the major axis with increasing axial ratio because it becomes increasingly difficult to set up a significant polarization electric field along the major axis. Consequently, the electric field that moves the elongated bubble becomes essentially that which moves the bulk plasma, the large-scale applied electric field. We conclude, therefore, that the observations of eastward plume drifts that are comparable to the eastward neutral winds indirectly supports the conclusion that plasma bubbles are vertically elongated upwellings.

The discussion presented above should not be interpreted to mean that the percentage depletion of a bubble does not influence its motion and growth direction. We have simply argued that the depletion

amount does not dominate the magnitude of eastward drift and have used this information to infer a bubble shape. Bubble depletions very likely produce the tilts of plumes as originally proposed by Woodman and LaHoz [1976].

Other results extracted from the analysis presented here provide further evidence in support of the hypothesis that an eastward neutral wind plays an important role in the ESF structuring process. Tsunoda [1981] suggested that the west wall of altitude-modulated regions in the bottomside F layer was probably gradient-drift unstable because of the presence of an eastward neutral wind. Tsunoda and White [1981] demonstrated that altitude-modulation of constant plasma-density contours actually exist in the bottomside F layer prior to ESF backscatter formation, and that plumes develop from the crests of these large-scale upwellings. Tsunoda et al. [1981] also showed that a velocity shear (with altitude) in east-west plasma drift existed in the bottomside F layer that enhanced the growth rate of the gradient-drift instability by increasing the relative velocity between the plasma and the neutral gas. The results presented in the previous section showed the actual development of plumes from the west wall of the large-scale altitude modulations while the east wall remained relatively structureless.

REFERENCES

Chaturvedi, P. K., and S. L. Ossakow, "Nonlinear theory of the collisional Rayleigh-Taylor instability in equatorial spread F," J. Geophys. Res., 83, 4219, 1978.

Farley, D. T., "A theory of electrostatic fields in the ionosphere at nonpolar geomagnetic latitudes," J. Geophys. Res., 65, 869, 1960.

Fejer, B. G., D. T. Farley, C. A. Gonzales, R. F. Woodman, and C. Calderon, "F region east-west drifts at Jicamarca," J. Geophys. Res., 86, 215, 1981.

Hanson, W. B., and R. A. Heelis, "Techniques for measuring bulk gas-motions from satellites," Space Sci. Instr., 1, 493, 1975.

Hanson, W. B., and S. Sanatani, "Large Ni gradients below the equatorial-F peak," J. Geophys. Res., 78, 1167, 1973.

Huba, J. D., P. K. Chaturvedi, S. L. Ossakow, and D. M. Towle, "High-frequency drift waves with wavelengths below the ion gyroradius in equatorial spread F," Geophys. Res. Letts., 5, 695, 1978.

Huba, J. D., and S. L. Ossakow, "On 11-cm irregularities during equatorial spread F," J. Geophys. Res., 86, 829, 1981.

Hudson, M. K., "Spread F bubbles: nonlinear Rayleigh-Taylor mode in two dimensions," J. Geophys. Res., 83, 3189, 1978.

Kelley, M. C., and E. Ott, "Two-dimensional turbulence in equatorial spread F," J. Geophys. Res., 83, 4369, 1978.

Kelley, M. C., G. Haerendel, H. Kappler, A. Valenzuela, B. B. Balsley, D. A. Carter, W. L. Ecklund, C. W. Carlson, B. Hausler, and R. Torbert, "Evidence for a Rayleigh-Taylor-type instability and upwelling of depleted density regions during equatorial spread F," Geophys. Res. Letts., 3, 448, 1976.

McClure, J. P., W. B. Hanson, and J. H. Hoffman, "Plasma bubbles and irregularities in the equatorial ionosphere," J. Geophys. Res., 82, 2650, 1977.

Morse, F. A., B. C. Edgar, H. C. Koons, C. J. Rice, W. H. Heikkila, J. H. Hoffman, B. A. Tinsley, J. D. Winningham, A. B. Christensen, R. F. Woodman, J. Pomalaza, and N. R. Teixeira, "Equion, an equatorial ionospheric irregularity experiment," J. Geophys. Res., 82, 578, 1977.

Ossakow, S. L., and P. K. Chaturvedi, "Morphological studies of rising equatorial spread-F bubbles," J. Geophys. Res., 83, 2085, 1978.

Ossakow, S. L., S. T. Zalesak, B. E. McDonald, and P. K. Chaturvedi, "Nonlinear equatorial spread F: dependence on altitude of the F peak and bottomside background electron density gradient scale length," J. Geophys. Res., 84, 17, 1979.

Ott, E., "Theory of Rayleigh-Taylor bubbles in the equatorial ionosphere," J. Geophys. Res., 83, 2066, 1978.

Rishbeth, H., "Polarization fields produced by winds in the equatorial F region," Planet Space Sci., 19, 357, 1971.

Scannapieco, A. J., and S. L. Ossakow, "Nonlinear equatorial spread F," Geophys. Res. Letts., 3, 451, 1976.

Sipler, D. P., and M. A. Biondi, "Equatorial F-region neutral winds from nightglow OI 630.0 nm Doppler shifts," Geophys. Res. Letts., 5, 373, 1978.

Sperling, J. L., and S. R. Goldman, "Electron collisional effects of lower hybrid drift instabilities in the ionosphere," J. Geophys. Res., 85, 3494, 1980.

Szuszczewicz, E. P., R. T. Tsunoda, R. Narcisi, and J. C. Holmes, "Coincident radar and rocket observations of equatorial spread F," Geophys. Res. Letts., 7, 537, 1980.

Towle, D. M., "VHF and UHF radar observations of equatorial ionospheric irregularities and background densities," Radio Sci., 15, 71, 1980.

Tsunoda, R. T., "Magnetic-field-aligned characteristics of plasma bubbles in the nighttime equatorial ionosphere," J. Atmos. Terr. Phys., 42, 743, 1980(a).

Tsunoda, R. T., "On the spatial relationship of 1-meter equatorial spread-F irregularities and plasma bubbles," J. Geophys. Res., 85, 185, 1980(b).

Tsunoda, R. T., "The growth and decay of equatorial backscatter plumes," Topical Report 4, Contract DNA001-79-C-0153, SRI Project 8164, SRI International, Menlo Park, CA 1980(c).

Tsunoda, R. T., "Time evolution and dynamics of equatorial backscatter plumes--1. Growth Phase," J. Geophys. Res., 86, 139, 1981.

Tsunoda, R. T., and D. P. Towle, "On the spatial relationship of 1-meter equatorial spread-F irregularities and depletions in total electron content," Geophys. Res. Lett., 6, 873, 1979.

Tsunoda, R. T., M. J. Baron, J. Owen, and D. M. Towle, "ALTAIR: an incoherent scatter radar for equatorial spread-F studies," Radio Sci., 14, 1111, 1979.

Tsunoda, R. T., R. C. Livingston, and C. L. Rino, "Evidence of a velocity shear in bulk plasma motion associated with the post-sunset rise of the equatorial F layer," Geophys. Res. Lett. (accepted for publication, 1981).

Tsunoda, R. T., and B. R. White, "On the generation and growth of equatorial backscatter plumes--1. Wave structure in the bottom-side F layer," J. Geophys. Res. (accepted for publication, 1981).

Woodman, R. F., "East-west ionospheric drifts at the magnetic equator," Space Res. XII, 12, 969, 1972.

Woodman, R. F., and C. LaHoz, "Radar observations of F-region equatorial irregularities," J. Geophys. Res., 81, 5447, 1976.

Zalesak, S. T., and S. L. Ossakow, "Nonlinear equatorial spread F; spatially large bubbles resulting from large horizontal scale initial perturbations," J. Geophys. Res., 85, 2131, 1980.

DISTRIBUTION LIST

DEPARTMENT OF DEFENSE

Assistant Secretary of Defense
Comm, Cmd, Cont & Intell
ATTN: Dir of Intelligence Sys, J. Babcock

Command & Control Technical Center
ATTN: C-650, G. Jones
ATTN: C-312, R. Mason
3 cy ATTN: C-650, W. Heidig

Defense Communications Agency
ATTN: Code 480
ATTN: Code 480, F. Dieter
ATTN: Code 810, J. Barna
ATTN: Code 205
ATTN: Code 101B

Defense Communications Engineer Center
ATTN: Code R410, N. Jones
ATTN: Code R123

Defense Intelligence Agency
ATTN: DT-1B
ATTN: DB-4C, E. O'Farrell
ATTN: DB, A. Wise
ATTN: Dir
ATTN: DC-7B

Defense Nuclear Agency
ATTN: NAFD
ATTN: STNA
ATTN: RAEE
ATTN: NATD
3 cy ATTN: RAAE
4 cy ATTN: TITL

Defense Technical Information Center
12 cy ATTN: DD

Field Command
Defense Nuclear Agency
ATTN: FCP

Field Command
Defense Nuclear Agency
Livermore Branch
ATTN: FCPRL

Interservice Nuclear Weapons School
ATTN: TTV

Joint Chiefs of Staff
ATTN: C3S, Evaluation Office
ATTN: C3S

Joint Strat Tgt Planning Staff
ATTN: JLA
ATTN: JLTW-2

National Security Agency
ATTN: R-52, J. Skillman
ATTN: B-3, F. Leonard
ATTN: W-32, O. Bartlett

Under Secretary of Defense for Rsch & Engrg
ATTN: Strategic & Space Sys (OS)

DEPARTMENT OF DEFENSE (Continued)

WWMCCS System Engineering Org
ATTN: R. Crawford

DEPARTMENT OF THE ARMY

Assistant Chief of Staff for Automation & Comm
Department of the Army
ATTN: DAAC-ZT, P. Kenny

Atmospheric Sciences Laboratory
U.S. Army Electronics R&D Command
ATTN: DELAS-EO, F. Niles

BMD Advanced Technology Center
Department of the Army
ATTN: ATC-T, M. Capps
ATTN: ATC-O, W. Davies

BMD Systems Command
Department of the Army
2 cy ATTN: BMDSC-HW

Deputy Chief of Staff for Ops & Plans
Department of the Army
ATTN: DAMO-RQC

Harry Diamond Laboratories
Department of the Army
ATTN: DELHD-I-TL, M. Weiner
ATTN: Chief, Div 20000
ATTN: DELHD-N-RB, R. Williams

U.S. Army Chemical School
ATTN: ATZN-CM-CS

U.S. Army Comm-Elec Engrg Instal Agency
ATTN: CCC-EMEO-PED, G. Lane
ATTN: CCC-CED-CCO, W. Neuendorf

U.S. Army Communications Command
ATTN: CC-OPS-W
ATTN: CC-OPS-WR, H. Wilson

U.S. Army Communications R&D Command
ATTN: DRDCO-COM-RY, W. Kesselman

U.S. Army Foreign Science & Tech Ctr
ATTN: DRXST-SD

U.S. Army Materiel Dev & Readiness Cmd
ATTN: DRCLDC, J. Bender

U.S. Army Missile Intelligence Agency
ATTN: YSE, J. Gamble

U.S. Army Nuclear & Chemical Agency
ATTN: Library

U.S. Army Satellite Comm Agency
ATTN: Document Control

U.S. Army TRADOC Sys Analysis Actvy
ATTN: ATAA-PL
ATTN: ATAA-TDC
ATTN: ATAA-TCC, F. Payan, Jr

DEPARTMENT OF THE NAVY

COMSPTEVFOR
Department of the Navy
ATTN: Code 605, R. Berg

Joint Cruise Missiles Project Ofc
Department of the Navy
ATTN: JCMG-707

Naval Air Development Center
ATTN: Code 6091, M. Setz

Naval Air Systems Command
ATTN: PMA 271

Naval Electronic Systems Command
ATTN: PME 117-211, B. Kruger
ATTN: PME 106-4, S. Kearney
ATTN: PME 106-13, T. Griffin
ATTN: PME 117-2013, G. Burnhart
ATTN: Code 501A
ATTN: PME 117-20
ATTN: Code 3101, T. Hughes

Naval Intelligence Support Ctr
ATTN: NISC-50

Naval Ocean Systems Center
ATTN: Code 532, R. Pappert
ATTN: Code 532, J. Bickel
ATTN: Code 5322, M. Paulsen
3 cy ATTN: Code 5323, J. Ferguson

Naval Research Laboratory
ATTN: Code 4780, S. Brown
ATTN: Code 7950, J. Goodman
ATTN: Code 7550, J. Davis
ATTN: Code 4187
ATTN: Code 4700, T. Coffey
ATTN: Code 7500, B. Wald

Naval Space Surveillance System
ATTN: J. Burton

Naval Surface Weapons Center
ATTN: Code F31

Naval Telecommunications Command
ATTN: Code 341

Office of Naval Research
ATTN: Code 420
ATTN: Code 465
ATTN: Code 421

Office of the Chief of Naval Operations
ATTN: OP 981N
ATTN: OP 941D
ATTN: OP 65

Strategic Systems Project Office
ATTN: NSP-2141
ATTN: NSP-43
ATTN: NSP-2722, F. Wimberly

DEPARTMENT OF THE AIR FORCE

Aerospace Defense Command
Department of the Air Force
ATTN: DC, T. Long

DEPARTMENT OF THE AIR FORCE (Continued)

Air Force Geophysics Laboratory
ATTN: OPR, H. Gardiner
ATTN: OPR-1
ATTN: LKB, K. Champion
ATTN: OPR, A. Stair
ATTN: S. Basu
ATTN: PHP
ATTN: PHI, J. Buchau
ATTN: R. Thompson

Air Force Weapons Laboratory
Air Force Systems Command
ATTN: SUL
ATTN: NTYC
ATTN: NTN

Air Force Wright Aeronautical Lab
ATTN: W. Hunt
ATTN: A. Johnson

Air Logistics Command
Department of the Air Force
ATTN: OO-ALC/MM

Air University Library
Department of the Air Force
ATTN: AUL-LSE

Air Weather Service, MAC
Department of the Air Force
ATTN: DNXP, R. Babcock

Assistant Chief of Staff
Studies & Analyses
Department of the Air Force
ATTN: AF/SASC, C. Rightmeyer
ATTN: AF/SASC, W. Keaus

Ballistic Missile Office
Air Force Systems Command
ATTN: ENSN, J. Allen

Deputy Chief of Staff
Operations Plans and Readiness
Department of the Air Force
ATTN: AFXOKS
ATTN: AFXOXFD
ATTN: AFXOKT
ATTN: AFXOKCD

Deputy Chief of Staff
Research, Development, & Acq
Department of the Air Force
ATTN: AFRDS
ATTN: AFRDSP
ATTN: AFRDSS

Electronic Systems Division
ATTN: DCKC, J. Clark

Electronic Systems Division
ATTN: OCT-4, J. Deas

Electronic Systems Division
ATTN: YSM, J. Kobelski
ATTN: YSEA

DEPARTMENT OF THE AIR FORCE (Continued)

Foreign Technology Division
Air Force Systems Command
ATTN: TQTD, B. Ballard
ATTN: NIIS, Library

Headquarters Space Division
Air Force Systems Command
ATTN: SKA, D. Bolin
ATTN: SKY, C. Kennedy

Headquarters Space Division
Air Force Systems Command
ATTN: YZJ, W. Mercer

Headquarters Space Division
Air Force Systems Command
ATTN: E. Butt

Rome Air Development Center
Air Force Systems Command
ATTN: OCS, V. Coyne
ATTN: TSLD

Rome Air Development Center
Air Force Systems Command
ATTN: EEP

Strategic Air Command
Department of the Air Force
ATTN: DCXT
ATTN: DCXR, T. Jorgensen
ATTN: NRT
ATTN: XPFS
ATTN: DCX

OTHER GOVERNMENT AGENCIES

Central Intelligence Agency
ATTN: OSWR/NED

Department of Commerce
National Bureau of Standards
ATTN: Sec Ofc for R. Moore

Department of Commerce
National Oceanic & Atmospheric Admin
ATTN: R. Grubb

Institute for Telecommunications Sciences
National Telecommunications & Info Admin
ATTN: A. Jean
ATTN: L. Berry
ATTN: W. Utlaut

DEPARTMENT OF ENERGY CONTRACTORS

EG&G, Inc
Los Alamos Division
ATTN: J. Colvin
ATTN: D. Wright

Lawrence Livermore National Lab
ATTN: L-389, R. Ott
ATTN: L-31, R. Hager
ATTN: Technical Info Dept, Library

DEPARTMENT OF ENERGY CONTRACTORS (Continued)

Los Alamos National Laboratory
ATTN: D. Simons
ATTN: E. Jones
ATTN: D. Westervelt
ATTN: P. Keaton
ATTN: MS 670, J. Hopkins
ATTN: R. Taschek
ATTN: MS 664, J. Zinn

Sandia Laboratories
Livermore Laboratory
ATTN: B. Murphey
ATTN: T. Cook

Sandia National Lab
ATTN: ORG 4241, T. Wright
ATTN: D. Thornbrough
ATTN: ORG 1250, W. Brown
ATTN: 3141
ATTN: D. Dahlgren
ATTN: Space Project Div

DEPARTMENT OF DEFENSE CONTRACTORS

Aerospace Corp
ATTN: R. Slaughter
ATTN: J. Straus
ATTN: V. Josephson
ATTN: I. Garfunkel
ATTN: D. Olsen
ATTN: T. Salmi
ATTN: N. Stockwell
ATTN: S. Bower

University of Alaska
ATTN: Technical Library
ATTN: N. Brown
ATTN: T. Davis

Analytical Systems Engineering Corp
ATTN: Radio Sciences

Analytical Systems Engineering Corp
ATTN: Security

Barry Research Corporation
ATTN: J. McLaughlin

BDM Corp
ATTN: L. Jacobs
ATTN: T. Neighbors

Berkeley Research Associates, Inc
ATTN: J. Workman

Betac
ATTN: J. Hirsch

Boeing Co
ATTN: M/S 42-33, J. Kennedy
ATTN: G. Hall
ATTN: S. Tashird

Booz-Allen & Hamilton, Inc
ATTN: B. Wilkinson

DEPARTMENT OF DEFENSE CONTRACTORS (Continued)

University of California at San Diego
ATTN: H. Booker

Charles Stark Draper Lab, Inc
ATTN: J. Gilmore
ATTN: D. Cox

Communications Satellite Corp
ATTN: D. Fang

Computer Sciences Corp
ATTN: F. Eisenbarth

Comsat Labs
ATTN: R. Taur
ATTN: G. Hyde

Cornell University
ATTN: M. Kelly
ATTN: D. Farley, Jr

E-Systems, Inc
ATTN: R. Berezdivin

Electrospace Systems, Inc
ATTN: H. Logston

ESL, Inc
ATTN: J. Marshall

General Electric Co
ATTN: M. Bortner
ATTN: A. Harcar

General Electric Co
ATTN: C. Zierdt
ATTN: A. Steinmayer

General Electric Co
ATTN: F. Reibert

General Electric Co
ATTN: G. Millman

General Research Corp
ATTN: J. Ise, Jr
ATTN: J. Garbarino

Harris Corp
ATTN: E. Knick

Horizons Technology, Inc
ATTN: R. Kruger

HSS, Inc
ATTN: D. Hansen

IBM Corp
ATTN: F. Ricci

University of Illinois
ATTN: K. Yeh

Institute for Defense Analyses
ATTN: E. Bauer
ATTN: H. Wolfhard
ATTN: J. Aein
ATTN: J. Bengston

DEPARTMENT OF DEFENSE CONTRACTORS (Continued)

International Tel & Telegraph Corp
ATTN: Technical Library
ATTN: G. Wetmore

JAYCOR
ATTN: J. Sperling

JAYCOR
ATTN: J. Doncarlos

Johns Hopkins University
ATTN: T. Potemra
ATTN: J. Phillips
ATTN: T. Evans
ATTN: J. Newland
ATTN: P. Komiske

Kaman Tempo
ATTN: DASIAC
ATTN: T. Stephens
ATTN: W. McNamara
ATTN: W. Knapp

Linkabit Corp
ATTN: I. Jacobs

Litton Systems, Inc
ATTN: R. Grasty

Lockheed Missiles & Space Co, Inc
ATTN: W. Imhof
ATTN: M. Walt
ATTN: R. Johnson

Lockheed Missiles & Space Co, Inc
ATTN: Dept 60-12
ATTN: D. Churchill
ATTN: C. Old

M.I.T. Lincoln Lab
ATTN: D. Towle

Martin Marietta Corp
ATTN: R. Heffner

McDonnell Douglas Corp
ATTN: N. Harris
ATTN: J. Moule
ATTN: W. Olson
ATTN: G. Mroz
ATTN: R. Halprin

Meteor Communications Consultants
ATTN: R. Leader

Mission Research Corp
ATTN: R. Kilb
ATTN: Tech Library
ATTN: R. Hendrick
ATTN: F. Fajen
ATTN: R. Bogusch
ATTN: S. Gutsche
ATTN: D. Sappenfield

Mitre Corp
ATTN: G. Harding
ATTN: C. Callahan
ATTN: A. Kymmel
ATTN: B. Adams

DEPARTMENT OF DEFENSE CONTRACTORS (Continued)

Mitre Corp
ATTN: M. Horrocks
ATTN: W. Foster
ATTN: J. Wheeler
ATTN: W. Hall

Pacific-Sierra Research Corp
ATTN: F. Thomas
ATTN: E. Field, Jr
ATTN: H. Brode

Pennsylvania State University
ATTN: Ionospheric Research Lab

Photometrics, Inc
ATTN: I. Kofsky

Physical Dynamics, Inc
ATTN: E. Fremouw

Physical Research, Inc
ATTN: R. Deliberis

R & D Associates
ATTN: R. Lelevier
ATTN: R. Turco
ATTN: C. Greifinger
ATTN: B. Gabbard
ATTN: M. Gantsweg
ATTN: W. Karzas
ATTN: H. Ory
ATTN: W. Wright
ATTN: F. Gilmore
ATTN: P. Haas

R & D Associates
ATTN: B. Yoon

Rand Corp
ATTN: E. Bedrozian
ATTN: C. Crain

Riverside Research Institute
ATTN: V. Trapani

Rockwell International Corp
ATTN: R. Buckner

Rockwell International Corp
ATTN: S. Quilici

DEPARTMENT OF DEFENSE CONTRACTORS (Continued)

Santa Fe Corp
ATTN: D. Paolucci

Science Applications, Inc
ATTN: E. Straker
ATTN: L. Linson
ATTN: C. Smith
ATTN: D. Hamlin

Science Applications, Inc
ATTN: SZ

Science Applications, Inc
ATTN: J. Cockayne

SRI International
ATTN: R. Leadabrand
ATTN: D. Neilson
ATTN: J. Petrickes
ATTN: C. Rino
ATTN: G. Price
ATTN: A. Burns
ATTN: M. Baron
ATTN: G. Smith
ATTN: W. Chesnut
ATTN: W. Jaye
4 cy ATTN: R. Livingston
4 cy ATTN: R. Tsunoda

Sylvania Systems Group
ATTN: I. Kohlberg
ATTN: R. Steinhoff

Technology International Corp
ATTN: W. Boquist

Tri-Com, Inc
ATTN: D. Murray

TRW Defense & Space Sys Group
ATTN: R. Plebuch
ATTN: D. Dee

Utah State University
ATTN: K. Baker
ATTN: L. Jensen
ATTN: J. Dupnik

Visidyne, Inc
ATTN: C. Humphrey
ATTN: J. Carpenter


DAT
ILM